Available online at www.sciencedirect.com
SCIENCE DIRECT®
Journal of Solid State Chemistry 173 (2003) 476–488
JOURNAL OF SOLID STATE CHEMISTRY
http://elsevier.com/locate/jssc

$BaO–Nd_2O_3–CuO_x$ subsolidus equilibria under carbonate-free conditions at $pO_2 = 100\,Pa$ and at $pO_2 = 21\,kPa$

W. Wong-Ng,[a,*] L.P. Cook,[a] J. Suh,[b] R. Coutts,[b] J.K. Stalick,[a] I. Levin,[a] and Q. Huang[a]

[a] *Materials Science and Engineering Laboratory, NIST, Gaithersburg, MD 20899, USA*
[b] *Geology Department, University of Maryland, College Park, MD 20749, USA*

Received 18 April 2002; received in revised form 19 December 2002; accepted 7 January 2003

Abstract

Subsolidus phase equilibria of the $BaO–Nd_2O_3–CuO_x$ system at $pO_2 = 100\,Pa$ (0.1% O_2 volume fraction, 810°C) and at $pO_2 = 21\,kPa$ (21% O_2 volume fraction, 930°C) have been investigated by applying controlled-atmosphere methods to minimize the presence of carbonate and CO_2 and H_2O contamination. Under carbonate-free conditions, the $BaO–Nd_2O_3–CuO_x$ phase diagrams at $pO_2 = 100\,Pa$ and at $pO_2 = 21\,kPa$ are similar to one another except for differences in the extent of the solid solutions. Apart from the limiting binary phases, the ternary system consists of three solid solutions and one stoichiometric ternary compound. The first solid solution is the high T_c series, $Ba_{2-x}Nd_{1+x}Cu_3O_{6+z}$ ($0.3 \geqslant x \geqslant 0$ at $pO_2 = 100\,Pa$; $0.95 \geqslant x \geqslant 0$ at $pO_2 = 21\,kPa$). At $pO_2 = 21\,kPa$, a compositionally dependent phase change was detected, from tetragonal ($0.7 > x \geqslant 0$) to orthorhombic ($0.95 \geqslant x \geqslant 0.7$). The second solid solution series, the 'brown-phase' $Ba_{1+x}Nd_{2-x}CuO_z$, has a narrow homogeneity region ($0.10 > x \geqslant 0$ at $pO_2 = 100\,Pa$; $0.15 > x \geqslant 0$ at $pO_2 = 21\,kPa$). In the high BaO part of the phase diagram, a third solid solution ($Ba_{2-x}Nd_x$)CuO_{3+z} ($x = 0$ to ≈ 0.3 at $pO_2 = 100\,Pa$; $x = 0-0.45$ at $pO_2 = 21\,kPa$) was confirmed, as well as a nominally stoichiometric phase, $Ba_4Nd_2Cu_2O_z$. The latter phase is an insulator, with a structure comprised of unusual CuO_5 linear chains. A significant difference in tie line distribution involving the $Ba_{2-x}Nd_{1+x}Cu_3O_{6+z}$ superconductor was found under carbonate-free conditions relative to literature studies completed in air. Instead of the $BaCuO_{2+x}–Ba_{2+x}Nd_{4-x}Cu_2O_z$ tie line normally encountered in air, a $Ba_{2-x}Nd_{1+x}Cu_3O_{6+z}–(Ba,Nd)_2CuO_{3+x}$ tie line was established. This tie line substantially expands the field of stability of the $Ba_{2-x}Nd_{1+x}Cu_3O_{6+z}$ superconductor phase into the BaO-rich region of the phase diagram. Implications for the processing of materials based on the $Ba_{2-x}Nd_{1+x}Cu_3O_{6+z}$ superconductor are discussed.

1. Introduction

The recent success of the rolling-assisted biaxially textured substrate (RABiTS [1–3]) and ion-beam-assisted deposition (IBAD [4,5]) processes in preparing $Ba_2RCu_3O_{6+z}$ (R-213)-based coated conductor materials with improved superconducting properties has stimulated reinvestigation of $BaO–R_2O_3–CuO_x$ systems (R = lanthanides and Y). In particular, the $BaO–Nd_2O_3–CuO_x$ system is one of the most promising lanthanide systems for the development of this second generation of high T_c materials. For example, the $Ba_2NdCu_3O_{6+x}$ (Nd-213) superconductor demonstrates a high T_c value (i.e. 94.5 K [6]) and enhanced vortex-pinning by comparison with $Ba_2YCu_3O_{6+x}$ (Y-213), resulting in higher critical current density and higher irreversibility field for bulk materials [7–9]. A substitution of Nd for Ba expands the range of solid solution (Nd-213ss), and physical properties can be controlled by varying the solid solution composition according to the formula $Ba_{2-x}Nd_{1+x}Cu_3O_{6+z}$. The considerably higher melting temperature of Nd-213 as compared with that of the Y-213 system [10] provides additional engineering benefits. For example, Y-213 can be used as a joining agent between two higher melting point R-213 materials [6].

Phase diagrams provide the basis for processing of Nd-213 materials, including the use of the melt-growth method [11,12]. A number of studies pertaining to the $BaO–Nd_2O_3–CuO_x$ phase equilibria [13–29] have been reported; however, they cannot be interpreted using a single-phase diagram. A majority of the data were collected using $BaCO_3$ as a starting reagent [11,15,17,22–24]. Other reported Ba-containing starting

*Corresponding author. Fax: +1-301-975-5334.
E-mail address: winnie.wong-ng@nist.gov (W. Wong-Ng).

0022-4596/03/$ - see front matter © 2003 Elsevier Science (USA). All rights reserved.
doi:10.1016/S0022-4596(03)00044-6

reagents include BaO_2 [14], BaO and $Ba(NO_3)_2$ [16]; however, most of the reported data was not collected entirely under controlled-atmosphere conditions. As a result, the presence of carbonate or hydroxide in the samples has rendered phase diagram determinations in the high-BaO region tentative, and the reported diagrams are incomplete.

This paper is a part of a continuing effort to understand the phase equilibria and crystal chemistry of AO–R_2O_3–CuO_x systems (A = alkaline earths). Since the crystal chemistry of relevant compounds has been discussed in our previous paper [17], the present paper will concentrate on the completion of the R = Nd phase diagram using BaO-derived starting materials. Particular emphasis is placed on the region near the BaO corner, and on the solid solution formation in $Ba_{2-x}Nd_{1+x}Cu_3O_{6+z}$ and its tie-line relationships with neighboring compounds. This work has utilized special experimental procedures to eliminate the presence of carbonate and minimize exposure to atmospheric CO_2 and moisture. Experimental work was carried out at two oxygen pressures, namely, at $pO_2 = 100$ Pa (0.1% O_2 in Ar volume fraction) and at $pO_2 = 21$ kPa (21% O_2 in Ar volume fraction). The former pO_2 was selected to approximate IBAD and RABiTS processing conditions.

2. Experimental[1]

2.1. Sample preparation and annealing

A solid-state reaction technique was employed for sample preparation. Since the commercial Nd_2O_3 powder used for this study (99.9% mass fraction purity, metals basis) reacts readily with atmospheric moisture to form $Nd(OH)_3$, a preliminary heat-treatment at 450°C was necessary to convert hydroxide into oxide prior to sample preparation. BaO was prepared by decomposing $BaCO_3$ (99.99% mass fraction purity, metals basis) at 1300°C in a vacuum furnace, and was then transferred to an Ar-filled glovebox using a sealed transfer vessel. The production of single-phase BaO was demonstrated by powder X-ray diffraction, as shown in Fig. 1. After weighing and homogenization of individual compositions prepared from BaO, Nd_2O_3 and CuO (99.99% mass fraction purity, metals basis), pellets were pressed and placed inside individual MgO crucibles, and then transferred to a controlled-atmosphere annealing furnace using another transfer vessel and an interlock system. A total of 71 samples each was prepared for this study (as listed in Table 1). Experiments were conducted at $pO_2 = 100$ Pa and at $pO_2 = 21$ kPa, as maintained by a mass flowmeter connected to cylinders of O_2 and Ar, and monitored by a zirconia oxygen sensor at both the gas inlet and the outlet of the furnace. For the experiments at $pO_2 = 100$ Pa, heat treatments were completed at 810°C, while for the experiments at $pO_2 = 21$ kPa, heat treatments were completed at 930°C. BaO-rich samples were equilibrated first at 750°C (100 Pa) and 900°C (21 kPa) prior to higher temperature annealings at 810°C and 930°C, respectively. Samples were cooled to room temperature at an approximate rate of 400°C/h. Several intermediate grindings and pressings took place until the content of the phase assemblages did not change, as determined from the results of powder X-ray diffraction. Experiments were also performed in which small samples of Nd-213ss were quenched into liquid nitrogen-cooled helium to study the crystal chemistry.

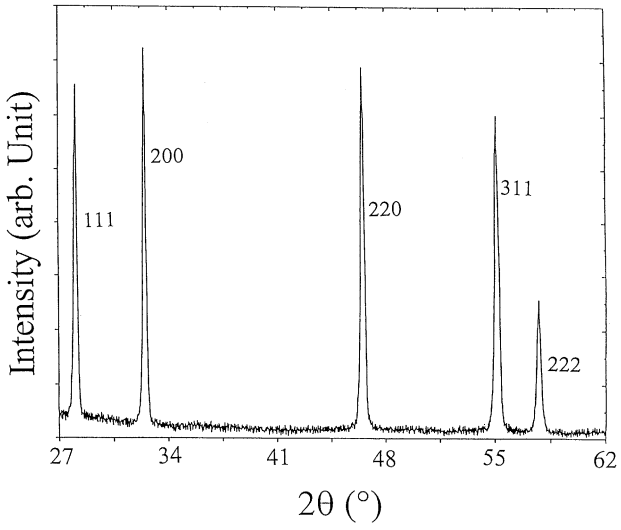

Fig. 1. X-ray diffraction pattern of single-phase BaO made using a sealed sample holder [30], demonstrating the absence of peaks due to $Ba(OH)_2$ and $BaCO_3$.

2.2. X-ray powder diffraction

For X-ray analysis, specimens were loaded into a sealed cell designed by Ritter [30]. The process of sample loading was performed inside an Ar-filled glovebox. X-ray powder diffraction was used to identify the phases synthesized, to confirm phase purity, and to determine the limit of solid solutions. Samples were analyzed using a computer-controlled automated diffractometer equipped with a theta-compensation slit; Cu$K\alpha$ radiation was used at 45 kV and 40 mA. The radiation was detected by a scintillation counter and a solid-state amplifier. A Siemens diffraction software package and reference X-ray diffraction patterns of the

[1] Certain trade names and company products are mentioned in the text or identified in illustrations in order to adequately specify the experimental procedure and equipment used. In no case does such identification imply recommendation or endorsement by National Institute of Standards and Technology.

Table 1
Compositions prepared for the phase diagram studies of the BaO–Nd_2O_3–CuO_x system at $pO_2 = 100$ Pa and at $pO_2 = 21$ kPa

Ba	Nd	Cu
36.67	13.33	50
35	15	50
34.17	15.83	50
33.33	16.67	50
31.67	18.33	50
30	20	50
28.33	21.67	50
26.67	23.33	50
25.00	25.00	50
23.33	26.67	50
21.67	28.33	50
20	30	50
18.33	31.67	50
16.67	33.33	50
3.33	63.33	33.33
27.85	48.10	24.05
30.77	46.15	23.08
36.67	13.33	50
50	25	25
50	12.50	37.50
60	10	30
66.67	0	33.33
60.00	6.67	33.33
53.33	13.33	33.33
46.67	20.00	33.33
34.17	15.83	50
45	10	45
60	10	30
25	5	70
10	30	60
15	40	45
25	35	40
20	70	10
55	35	10
65	15	20
10	65	25
15	10	75
30	55	15
5	45	50
2.5	47.5	50
30	45	25
32.5	42.5	25
65	5	30
40	25	35
25	46	29
37	42	21
32	10	58
44	17	39
20	53	27
60	15	25
60	13	27
57	13	30
63	9	28
60	7	33
60	20	20
70	8	22
63.5	5	31.5
55	5	40
45	15	40
45	45	10
66.66		33.34
20	35	45
13	22	65
55	30	15
44	36	20
59	9	32
18	35	47
65	8	27
27	36	37
15	55	30
50	10	40

ICDD powder diffraction file (PDF)[2] were used for phase identification.

2.3. Neutron diffraction studies

Neutron diffraction data for $BaNd_2O_4$ were collected using the 32-detector unit of the BT-1 diffractometer at the NIST NBSR research reactor. A Cu (311) monochromator ($\lambda = 1.5396(1)$ Å) was employed. Samples were loaded in a 6 mm diameter vanadium container, and measurements were made under ambient conditions. Additional details of the experimental setup can be found at http://www.ncnr.nist.gov.

2.4. Electron diffraction study

Specimens for transmission electron microscopy were prepared by grinding and polishing of the sintered pellets followed by dimpling up to a thickness of 30 mm. The thinning was accomplished in a Gatan precision ion-polishing system at a voltage of 5 kV. Some specimens were prepared by dispersing powder that had been crushed in acetone onto lacey-carbon-coated copper grids. The specimens were examined in a Phillips EM 430 transmission electron microscope operated at 200 kV.

3. Results and discussion

Figs. 2 and 3 give the ternary phase diagrams of BaO–Nd_2O_3–CuO_x prepared at $pO_2 = 100$ Pa (810°C), and at $pO_2 = 21$ kPa (930°C), respectively. The notation adopted for neodymium oxide is $\frac{1}{2}Nd_2O_3$, so that the composition ratio is the same as the cation ratio of the other end members in the system. The diagram prepared at $pO_2 = 21$ kPa is similar to that reported by Abbattista et al. [16] which was prepared under pure O_2.

[2] PDF, Powder Diffraction File, produced by International Centre for Diffraction Data (ICDD), 12 Campus Blvd., Newtown Square, PA. 19073–3273.

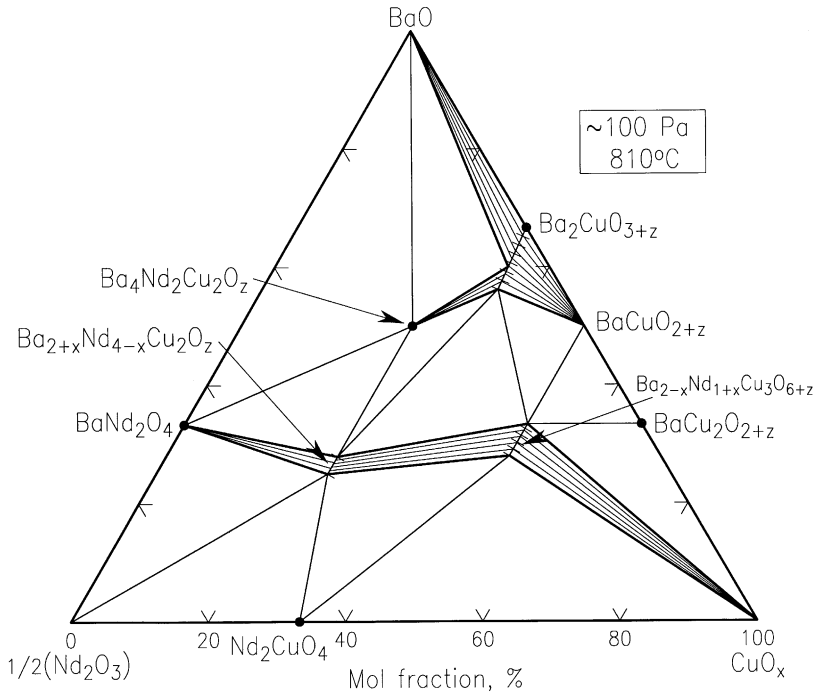

Fig. 2. Phase diagram of the $BaO–Nd_2O_3–CuO_x$ system prepared at $pO_2 = 100$ Pa.

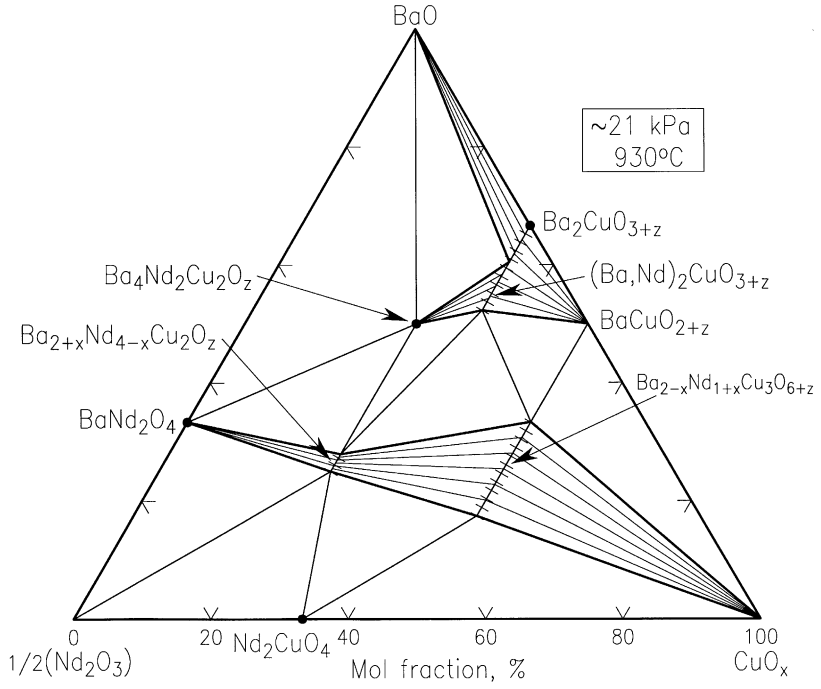

Fig. 3. Phase diagram of the $BaO–Nd_2O_3–CuO_x$ system prepared at $pO_2 = 21$ kPa.

BaO-rich samples, prepared without controlled atmosphere, are often contaminated with either CO_2 or moisture, and, therefore, phase formation is difficult to control, and the phase identification is complicated. In the present study under atmospheric-controlled conditions, both the solid solution $(Ba,Nd)_2CuO_{3+z}$ and the $Ba_4Nd_2Cu_2O_9$ phase were identified in the BaO-rich domain. However, many of the phases previously reported in the literature, when $BaCO_3$ was used, were not observed. For example, $Ba_3RCu_2O_z$, $Ba_4RCu_2O_z$, $Ba_5RCu_3O_z$ [31,32], $Ba_4RCu_3O_z$, $Ba_8R_3Cu_5O_z$ [33] and $Ba_6RCu_3O_z$ [24,34] were not observed regardless of the oxygen pressure. Fu et al. [18] reported that $BaNd_2CuO_z$ and Ba_2NdCuO_z are part of the same solid solution

series, rather than distinct phases. In the report by Hodorowicz et al. [19], there was no ternary compound near the BaO end, and instead of $BaNd_2CuO_5$ (brown phase), $BaNd_3CuO_z$ was observed.

The following discussion pertains to the phase equilibria and crystal chemistry of compounds in the ternary $BaO–Nd_2O_3–CuO_x$ system and its subsystems that were investigated at $pO_2 = 100$ Pa and at $pO_2 = 21$ kPa. Lattice parameters determined using X-ray diffraction are nominal values obtained using the sealed sample holder.

3.1. Limiting binary systems

3.1.1. The $BaO–Nd_2O_3$ system

In the binary $BaO–Nd_2O_3$ system, the only compound observed was $BaNd_2CuO_4$. The three other phases, $Ba_3R_4O_9$, $Ba_4R_2O_7$, and $Ba_2R_2O_5$, which have been reported elsewhere in the Y-containing analog [31], were not observed under carbonate-free conditions. This agrees with previous studies, which have established that '$Ba_4R_2O_7$' and '$Ba_2R_2O_5$' are oxycarbonates existing only in the presence of CO_2 [33]. The actual chemical formulas of these compounds can be written as $Ba_2R_2O_5 \cdot xCO_2$ and $Ba_4R_2O_7 \cdot xCO_2$.

3.1.1.1. Structure of $BaNd_2O_4$. The compound $BaNd_2O_4$ was found by neutron diffraction to be isostructural with BaY_2O_4 [35] and SrY_2O_4 [36], and the structure is of the $CaFe_2O_4$ type, with space group *Pnma* (No. 62 [37]). X-ray diffraction patterns of the BaR_2O_4 series have been reported by Wong-Ng et al. [38]. A projection of the $BaNd_2O_4$ structure along the *b*-axis is shown in Fig. 4. Table 2 gives the atomic coordinates and the displacement factors (thermal parameters). Table 3 gives the bond distances and bond valence sum values [39,40] of $BaNd_2O_4$. The lattice parameters of $BaNd_2O_4$ were determined to be $a = 10.58852(21)$ Å, $b = 3.60473(7)$ Å, $c = 12.4449(3)$ Å, and $Z = 4$. In the $BaNd_2O_4$ structure, Nd atoms are located inside distorted octahedra with two independent Nd ions (Nd1 and Nd2) in the asymmetric unit. A pair of $Nd(1)O_6$ octahedra share edges to form a structure motif, and motifs are connected by corner-sharing. Ba atoms are located in the octahedral tunnels formed by the $[NdO_6]$ units. The average Nd1-O and Nd2-O bond distances are 2.392 and 2.396 Å, respectively, which are in good agreement with those found in related compounds [41,42]. The distortion ratio (ratio of the shortest distance to the longest one) values of 0.955 and 0.955 do not deviate significantly from the ideal value of 1.0. Associated with each Nd1 and Nd2 are additional longer Nd–O distances of 3.881(3) and 3.521(3) Å, respectively. Therefore, the Nd atoms can be considered as having a (6 + 1) coordination. The bond valence sum values of Nd1 and Nd2 (2.889 and 2.840, respectively) are very close to the value of '3'. No significant residual bond strain was found associated with these polyhedral cages. The Ba–O distances range from 2.765(3) to 3.977(5) Å, giving rise to an average value of 2.982 Å and a rather large distortion ratio of 2.695. The bond valence value of Ba (1.8) is significantly smaller than the value of 2.0, indicating an underbonding, i.e. the size of the nine-coordinated cage is relatively large for Ba.

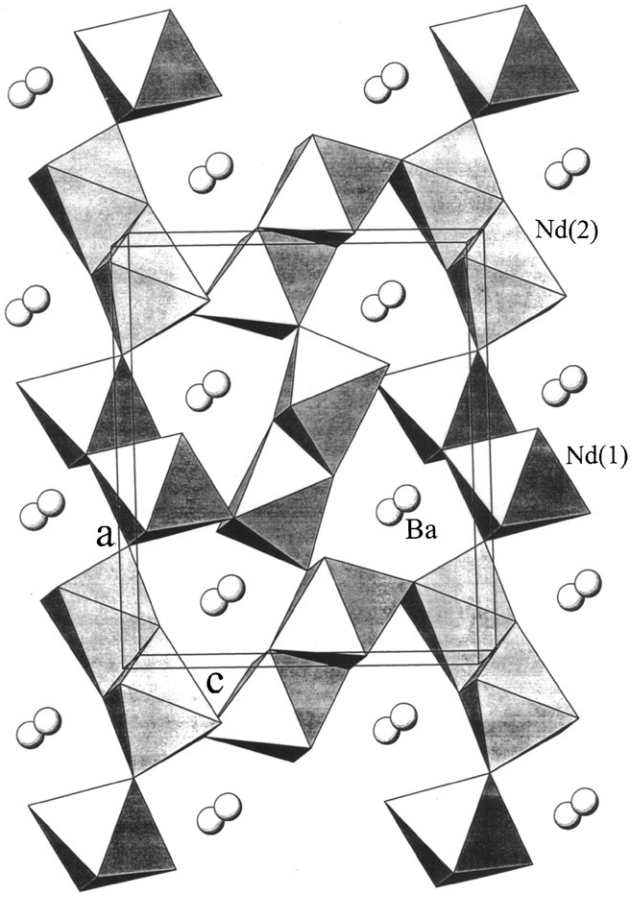

Fig. 4. Crystal structure of $BaNd_2O_4$.

Table 2
Atomic coordinates of $BaNd_2O_4$ from neutron Rietveld refinement

Atom	*x*	*y*	*z*	U_{iso}
Ba	0.75052(25)	1/4	0.64649(25)	0.0074(7)
Nd1	0.42409(23)	1/4	0.11243(15)	0.0042(5)
Nd2	0.41945(23)	1/4	0.61191(15)	0.0042(5)
O1	0.21283(24)	1/4	0.17142(23)	0.0095(7)
O2	0.12320(22)	1/4	0.48335(22)	0.0093(7)
O3	0.51418(25)	1/4	0.78210(21)	0.0114(7)
O4	0.42989(29)	1/4	0.42423(18)	0.0100(7)

The lattice parameters are: *Pnma* (No. 62), $a = 10.58852(21)$ Å, $b = 3.60473(7)$ Å, and $c = 12.4449(3)$ Å; $R_{wp} = 0.026$, $R_p = 0.021$, and $\chi^2 = 0.969$.

Table 3
Bond distances and bond valence found in $BaNd_2O_4$

M–O	Distance (Å)	M–O	Distance (Å)
Ba–O4 × 2	2.9213(35)	Nd1–O4	2.354(4)
–O4	3.977(5)	–O5	2.4219(34)
–O5 × 2	2.7654(27)	–O5 × 2	2.4657(25)
–O6	3.018(4)	–O6 × 2	2.3236(22)
–O6	2.930(4)	–O7	3.8809(31)
–O7 × 2	2.7699(28)	Ave.	2.6051
Ave.	2.9820	DR	0.9547
DR	0.6953	*V*	2.889
V	1.791		
Nd2–O4 × 2	2.3998(22)		
–O6	2.3434(33)		
–O7	2.3383(28)		
–O7 × 2	2.4486(27)		
–O5	3.5214(34)		
Ave.	2.3964		
DR	0.6640		
V	2.840		

DR = bond distortion ratio, V = bond valence sum (v.u.) [40,41].

3.1.2. The Nd_2O_3–CuO_x system

In the Nd_2O_3–CuO_x system at $pO_2 = 100$ Pa and at $pO_2 = 21$ kPa, the only phase observed was Nd_2CuO_4, which crystallizes with the *I*4/*mmm* symmetry [43] ($a = 3.945$ Å and $c = 12.171$ Å). The structure of Nd_2CuO_4 is different from that of La_2CuO_4 [44], which has a K_2NiF_4-type structure [45] (*Cmca*, $a = 5.363$ Å, $b = 5.409$ Å, and $c = 13.17$ Å). As the ionic radius of *R* decreases beyond Gd (Dy–Lu), the $R_2Cu_2O_5$ phase was found instead of R_2CuO_4 [46]. Under the present conditions, the reduced $RCuO_2$ phase, which was reported to be either hexagonal $P6_3/mmc$ [47] or rhombohedral $R3m$ [48], is not stable.

3.1.3. The BaO–CuO_x system

A review of the compounds in the BaO–CuO_x system was given by Wong-Ng and Cook [49]. As expected, samples prepared at $pO_2 = 21$ kPa contained two compounds: $BaCuO_{2+z}$ and Ba_2CuO_{3+z}. At $pO_2 = 100$ Pa an additional reduced phase, $BaCu_2O_{2+z}$, was observed. The oxygen content of the $BaCuO_{2+z}$ series has been reported to vary between 2.0 and 2.5. Three structure types are known ($0 < z < 0.12$, $0.29 < z < 0.36$, and $z = 0.5$). The most commonly recognized structural form of $BaCuO_{2+z}$ is cubic, with $0 < z < 0.12$. Phases with *x* greater than 0.12 have been reported by Petricek et al. [50].

The Ba_2CuO_{3zx} phase can only be prepared in a CO_2-free and moisture-free atmosphere [51]. Ba_2CuO_3 which is isostructural with Sr_2CuO_3 [52], has been reported to be either of the tetragonal or orthorhombic K_2NiF_4 type [45]. A phase transformation from orthorhombic (*Immm*) to tetragonal (*I*4/*mmm*) structure was reported to occur with decreasing oxygen content [14,16,27,53–55].

During studies of the BaO–Y_2O_3–CuO_x system, the reduced phase $BaCu_2O_{2+x}$ ($x \approx 0$) has often been observed in the crystallized quenched melt associated with melting reactions [56,57]. This phase was reported to be isostructural to $SrCu_2O_2$, which is tetragonal $I4_1/amd$ [58].

3.2. Ternary system BaO–Nd_2O_3–CuO_x

Determination of the phase diagram near the BaO corner is complicated not only by difficulty in removing all carbonate, but also by the hygroscopicity of BaO. Under the present experimental conditions, no melting occurred near the BaO region up to about 810°C at $pO_2 = 100$ Pa, and up to about 930°C at $pO_2 = 21$ kPa. Three solid solution series ($Ba_{2-x}Nd_{1+x}Cu_3O_{6+z}$, $Ba_{2-x}Nd_xCuO_{3+z}$, and $Ba_{1+x}Nd_{2-x}CuO_z$) and one nominally stoichiometric ternary oxide compound ($Ba_4Nd_2Cu_2O_9$ (422)) were observed in this system. The following discussion will include a brief review and the present results for these phases.

3.2.1. $Ba_{2-x}Nd_{1+x}Cu_3O_{6+z}$

3.2.1.1. Previous studies. Unlike Y-213, which forms a stoichiometric compound, the light rare-earth elements (R^{3+} from La to Gd) form a solid solution with the formula $Ba_{2-x}R_{1+x}Cu_3O_{6+z}$ (R-213ss) due to the substitution of R^{3+} into the Ba^{2+} sites [46,59–61]. For example, in the $Ba_{2-x}Nd_{1+x}Cu_3O_{6+z}$ (Nd-213ss) system, Nd^{3+} has an ionic radius (1.163 Å, IX-coordination [62,63]) approaching that of Ba^{2+} (1.47 Å, IX-coordination), which allows a large degree of solubility without forming second phases as compared with smaller cations such as Eu and Gd. The solid solution range of $Ba_{2-x}Nd_{1+x}Cu_3O_{6+z}$ has been reported to extend from $-0.05 < x < 1.0$ [21,29,64]; however, no clear consensus as to the extent of these solid solutions was established. In $Ba_{2-x}Nd_{1+x}Cu_3O_{6+z}$, both cation and oxygen non-stoichiometries are possible.

3.2.1.1.1. Oxygen non-stoichiometry. The oxygen non-stoichiometry of Nd-213ss has been studied intensively. For example, non-stoichiometric decomposition of Nd-123 as a function of *T* and pO_2 was reported by Lindemer et al. [26]. Studies of the effect of oxygen partial pressure on phase equilibria of the Nd-213 phase and the quasi-ternary phase diagram near the CuO region of the BaO–Nd_2O_3–CuO_x system have been conducted by Wu et al. [23,24], Yoshizumi et al. [65], and Yao et al. [83]. Goodilin et al. [64] studied the phase equilibria of the Nd-rich $Ba_{2-x}Nd_{1-x}Cu_3O_{6+z}$ solid solution, the melting equilibria and the limiting composition of the Nd-rich region. The lower solubility limit of Nd-213ss as a function of pO_2 was discussed by Wu et al. [24] who found that the solubility limit remains zero for

$pO_2 = 100$ Pa and $pO_2 = 1$ kPa, but narrows further with decreasing temperature.

3.2.1.1.2. Cation non-stoichiometry. $Ba_{2-x}Nd_{1+x}Cu_3O_{6+z}$ undergoes phase transitions as a result of Nd substitution into Ba, and also as a result of the variation of oxygen content [46]. According to Goodilin et al. [22], the solid solution $Ba_{2-x}Nd_{1+x}Cu_3O_{6+z}$ can be considered as consisting of three different compositional ranges: (1) $0.3 > z \geqslant 0.05$ (orthorhombic), (2) $0.6 > z \geqslant 0.3$ (tetragonal), and (3) $1.0 > z \geqslant 0.6$ (orthorhombic). At $z > 0.6$, ordering appears which leads to orthorhombic distortion of the tetragonal subcell. The observed superlattice ($a' = 2a, c' = 2c$) can be attributed to the ordering of Ba and Nd [66–70]. Petrykin et al. [70] reported Nd ordering in the face-centered (*Ammm*) superstructure. Additional oxygen atoms occupy vacant chain sites n the vicinity of barium atoms. Wong-Ng et al. [17] investigated the phase transition of $Ba_2RCu_3O_{6+z}$ in air as a function of the oxygen content z, and it was reported that lanthanide elements of smaller ionic size stabilize the orthorhombic phase at a higher temperature (or lower oxygen content). Powder X-ray diffraction study showed that the phase transformation between orthorhombic and tetragonal phases occurs between 570°C and 578°C.

3.2.1.1.3. Superconducting properties. The superconducting properties of $Ba_{2-x}Nd_{1+x}Cu_3O_{6+z}$ can be controlled in two ways, namely, by controlling the oxygen content, and also by varying the amount of substitution of Nd into Ba sites. Takekawa et al. [71], Yao and McCallum [72] studied the flux creep in $Ba_{2-x}Nd_{1+x}Cu_3O_{6+z}$, with $x = 0$–0.1. The correlation of hole filling, charge transfer and superconductivity was studied by Kramer et al. [59–61]. They established the dependence of T_c on x. Substitution of Nd introduces extra oxygen to maintain charge balance. This substitution results in a large amount of total oxygen in the sample (exceeding the value of 7). The extra oxygen consists of two parts: (i) the 'constituent oxygen' which neutralizes excess charge due to Nd substitution for Ba ($x/2$), and (ii) mobile oxygen which is exchangeable. The lowering of the T_c was attributed to the disruption of the CuO_4 chains, and to the introduction of extra oxygen into the anti-chains, which causes formation of more localized CuO_5 units. The combined effect is to decrease the amount of charge transfer to the CuO planes, thereby lowering the T_c values.

The possible pinning centers in the R-213 high T_c superconductors include twin planes, stacking faults, oxygen defects, dislocations and second phases. According to Murakami et al. [73], the $Ba_{2-x}Nd_{1+x}Cu_3O_{6+z}$ solid solution provides a new type of pinning center in melt grown samples when processed in reduced conditions. The critical current density (J_c) values of these samples are higher than that of the melt processed Y-213 with fine BaY_2CuO_5 inclusions. For example, one can utilize the fact that some members of the solid solution are not superconducting, and if they are finely distributed among a superconducting matrix, they can act as flux pinning agents under high field conditions [71].

3.2.1.2. Current results on solid solution extent. The tie-line distributions around the Nd-213 phase are indicated in Figs. 2 and 3. Nd-213 was found to have a large number of connecting tie-lines. No tie-line was observed between the 'brown' phase $Ba_{1+x}Nd_{2-x}CuO_z$ and $BaCuO_{2+x}$, which is in contrast to data collected using $BaCO_3$ as a starting reagent [21].

3.2.1.2.1. pO_2=100 Pa. The solid solution range for $Ba_{2-x}Nd_{1+x}Cu_3O_{6+z}$ samples prepared at $pO_2 = 100$ Pa, with $0.3 \geqslant x \geqslant 0$, is narrower than for those prepared under at $pO_2 = 21$ kPa or under oxygen. The liquid N_2/He quenched samples are tetragonal. The narrower solid solution range occurs because extra oxygen is needed to stabilize the solid solution members that are Nd-rich, and the oxygen partial pressure is not sufficient to stabilize such members [74]. The nominal lattice parameters of two members ($x = 0.1$ and 0.3) of this solid solution were determined. For $Ba_{1.9}Nd_{0.1}Cu_3O_{6+z}$, $a = 3.89863(3)$ Å, $c = 11.888(2)$ Å, $V = 180.48$ Å^3; for $Ba_{1.7}Nd_{0.3}Cu_3O_{6+z}$, $a = 3.8862(12)$ Å, $c = 11.861(4)$ Å, $V = 179.14$ Å^3. Similar to the solid solution series prepared at $pO_2 = 21$ kPa, the substitution of Nd for Ba correlates with the decrease of lattice parameters.

We noted that samples first processed at $pO_2 = 21$ kPa, then annealed at $pO_2 = 100$ Pa produced larger single-phase regions ($0.8 > x \geqslant 0$). Fig. 7 shows X-ray diffraction patterns for samples that have been equilibrated at $pO_2 = 21$ kPa at ≈ 930°C for approximately two weeks, and then heat-treated at $pO_2 = 100$ Pa for a further 3-week period, followed by slow-cooling. The $Ba_{1.1}Nd_{1.9}Cu_3O_{6+z}$ which was present in the specimen after treatment at $pO_2 = 21$ kPa, decomposed at $pO_2 = 100$ Pa (Fig. 5, $x = 0.9$). The final products contained two phases: tetragonal ($Ba_{2-x}Nd_{1+x}Cu_3O_{6+z}$, $0.7 > x \geqslant 0$, *P4/mmm*), and orthorhombic ($0.80 \geqslant x \geqslant 0.7$). These experiments illustrated that once the oxygen atoms are incorporated in the lattice of the R-213 materials, they are difficult to remove under relatively reducing conditions.

3.2.1.2.2. pO_2=21 kPa. At $pO_2 = 21$ kPa, the solid solution range 'x' of was confirmed to extend between $x = 0.0$ to nominally 0.95. X-ray diffraction patterns of $Ba_{2-x}Nd_{1+x}Cu_3O_{6+z}$, as quenched using flowing liquid nitrogen-cooled helium, are shown in Fig. 6. These patterns illustrate that single-phase Nd-213 was obtained. Lattice parameter determination (least-squares refinement program LSQ-NBS92 [75]) indicated that samples with $0 \leqslant x < 0.7$ are tetragonal. Peak splitting in the X-ray patterns was observed for samples with $x \geqslant 0.7$. We were able to index these patterns using the supercell reported by Abbattista et al. [16,27] and

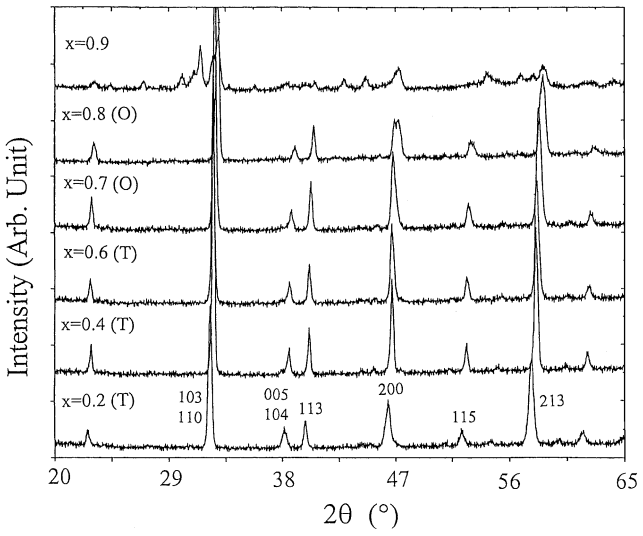

Fig. 5. X-ray diffraction patterns of the $Ba_{2-x}Nd_{1+x}Cu_3O_{6+z}$ series prepared at $pO_2 = 100$ Pa, after samples were initially prepared at $pO_2 = 21$ kPa, followed by heat-treatment at $pO_2 = 100$ Pa. Decomposition of $x = 0.9$ member is shown.

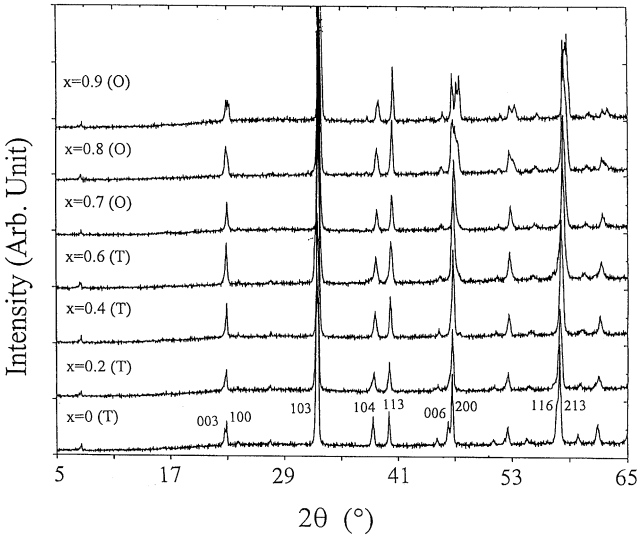

Fig. 6. X-ray diffraction patterns of the $Ba_{2-x}Nd_{1+x}Cu_3O_{6+z}$ series after annealing at $pO_2 = 21$ kPa at 930°C and quenching into helium gas cooled by liquid nitrogen.

Petrykin [70], namely, orthorhombic *Bmmm*, with $a' = 2a_T$, $b' = b_T$ and $c' = 2c_T$ (Table 4) where subscript T refers to the fundamental tetragonal unit cell. A plot of the unit-cell volume, V as a function of x in $Ba_{2-x}Nd_{1+x}Cu_3O_{6+z}$ is illustrated in Fig. 7. For the orthorhombic phases, the approximate subcell volumes (one-fourth of the volume of the supercell) are used. Since the size of Nd^{3+} is smaller than that of Ba^{2+} [62,63], a decrease of cell volume as a function of Nd substitution is observed. Two lines with different slope are inferred from Fig. 7, one corresponds to the tetragonal phase and the other to the orthorhombic phase.

Electron diffraction studies of the $Ba_{1.1}Nd_{0.9}Cu_3O_{6+z}$ specimen, sintered at 960°C and quenched in air, indicated orthorhombic superstructure with lattice parameters $a' = 2a_T$, $b' = 2b_T$ $(a<b)$, and $c' = 2c_T$ (Fig. 8). The observed set of reflection conditions is consistent with the three orthorhombic space groups: *Bbm*2 (No. 40), *Bbmm* (No. 63) and *Bb*2$_1$*m* (No. 36); the

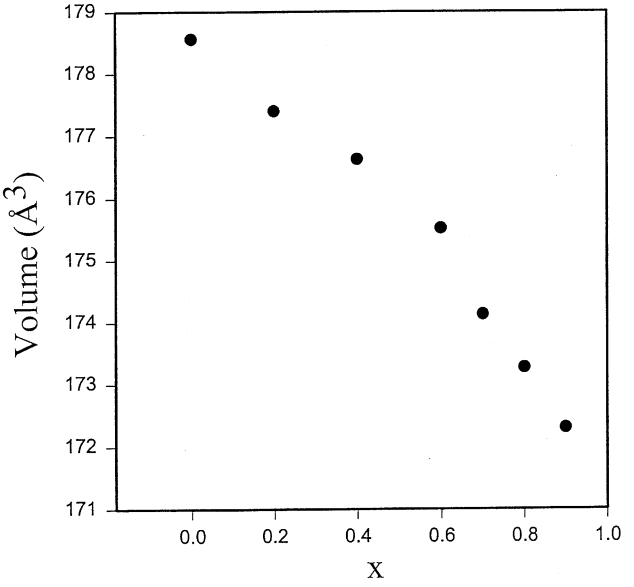

Fig. 7. Plots of unit-cell volume (V) against x in $Ba_{2-x}Nd_{1+x}Cu_3O_{6+z}$ (experiments at $pO_2 = 21$ kPa). For $0.95 \geqslant x \geqslant 0.7$, V of the tetragonal subcells were used.

Table 4
Nominal lattice parameters for $Ba_{2-x}Nd_{1+x}Cu_3O_{6+z}$ prepared at $pO_2 = 21$ kPa at 930°C and quenched in flowing liquid-nitrogen-cooled He

Composition	a (Å)	b (Å)	c (Å)	V (Å^3)
$Ba_{2.0}NdCu_3O_{6+z}$	3.8932(5)		11.7806(19)	178.56(4)
$Ba_{1.8}Nd_{1.2}Cu_3O_{6+z}$	3.8892(2)		11.7281(13)	177.40(2)
$Ba_{1.6}Nd_{1.4}Cu_3O_{6+z}$	3.8827(2)		11.6962(19)	176.32(2)
$Ba_{1.4}Nd_{1.6}Cu_3O_{6+z}$	3.883(5)		11.634(9)	175.52(4)
$Ba_{1.3}Nd_{1.7}Cu_3O_{6+z}$	3.8703(17)	7.778(3)	23.14(2)	174.13 [696.5(5)]
$Ba_{1.2}Nd_{1.8}Cu_3O_{6+z}$	3.8597(9)	7.769(3)	23.112(10)	173.27 [693.09(5)]
$Ba_{1.1}Nd_{1.9}Cu_3O_{6+z}$	3.8518(15)	7.765(4)	23.046(9)	172.34 [689.36(5)]

The volume (V) reported for compounds with $x = 0.7$, 0.8, and 0.9 corresponds to $\frac{1}{4}$ of the volume of the orthorhombic cell, as bracketed.

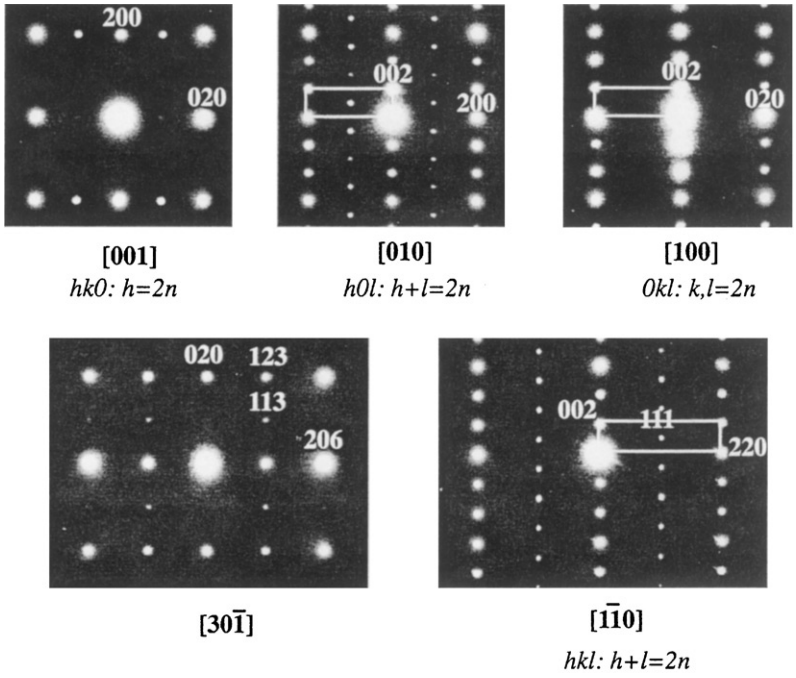

Fig. 8. SAD patterns of $Ba_{1.1}Nd_{1.9}Cu_3O_{6+z}$ prepared at $pO_2 = 21$ kPa at 930°C.

exact space group symmetry has yet to be determined. The superstructure is different from that reported by Goodilin et al. [22] by an additional doubling of the b_T-lattice parameter, bearing in mind that their specimens were prepared under different processing conditions. Apparently, the type of the superstructure developed is very sensitive to the processing details. In Fig. 3, it is possible that a small two-phase region exists between the tetragonal and orthorhombic phases. Based on our data, this region is rather narrow, and is confined within the composition range from $x = 0.6$ to 0.7 in $Ba_{2-x}Nd_{1+x}Cu_3O_{6+z}$. Currently we are in the process of characterizing the orthorhombic superstructure and the two-phase region in more detail using TEM.

We noted that for $Ba_{2-x}Nd_{1+x}Cu_3O_{6+z}$ samples that were slow-cooled at $pO_2 = 21$ kPa from ≈ 900°C, three different phases are discernible in the X-ray patterns [76]. Phase transformation occurred from the orthorhombic (O), ($0 < x \leqslant 0.2$, *Pmmm*), to tetragonal (T) phase, ($0.2 < x < 0.7$, *P4/mmm*), and then to another orthorhombic phase (O′), ($0.95 \geqslant x \geqslant 0.7$). This observation is in general agreement with the results of Goodilin et al. [22]. The difference in symmetry of these slow-cooled phases relative to that of the helium-quenched samples apparently results from the different oxygen content.

3.2.2. $Ba_{2-x}Nd_xCuO_{3+z}$

It was reported by Abbattista [16], and Zhang and Osamura [21] that under 100% by volume O_2 as well as in a mixture of ($21\%O_2 + Ar$), Nd substitutes for Ba in Ba_2CuO_{3+z} to form $Ba_{2-x}Nd_xCuO_{3+z}$ (x ranging from 0 to 0.5). This solid solution is stable in essentially carbonate-free systems only. According to Abbattista et al. [16], the $Ba_{2-x}Nd_xCuO_{3+z}$ phase shows tetragonal symmetry with a K_2NiF_4-type structure [45] at temperatures higher than 740°C. The low-temperature form is orthorhombic with a structure derived from that of Sr_2CuO_3. Under a reduced atmosphere (i.e. pO_2 of 10^{-6} atm) the Ba_2CuO_{3+z} phase becomes stoichiometric in oxygen (Ba_2CuO_3).

Our results confirmed existence of an appreciable solid solution range in $Ba_{2-x}Nd_xCuO_{3+z}$ when prepared at $pO_2 = 100$ Pa and at $pO_2 = 21$ kPa. We found that at $pO_2 = 21$ kPa, the x value was between 0 and 0.45, and at $pO_2 = 100$ Pa the value of x was smaller, between 0 and 0.3. The solid solution which was obtained after slow cooling can be indexed as an orthorhombic phase, *Immm*. The structure is of the Sr_2CuO_3 [52] or the Ca_2CuO_3 [77] type. The approximate lattice parameters for samples prepared at $pO_2 = 21$ kPa and at $pO_2 = 100$ Pa are listed in Table 5. Fig. 9 illustrates a plot of the unit-cell volume vs. x in $Ba_{2-x}Nd_xCuO_{3+z}$. A monotonic decrease of cell volume as a function of Nd substitution was again observed. It was also noted that, similar to $Ba_{2-x}Nd_{1+x}Cu_3O_{6+z}$, the solid solution extent was larger ($0.6 \geqslant x \geqslant 0$ in $Ba_{2-x}Nd_xCuO_{3+z}$) when samples were first prepared at $pO_2 = 21$ kPa prior to heat-treatments at $pO_2 = 100$ Pa.

3.2.3. $Ba_{1+x}Nd_{2-x}CuO_{5-z}$ (brown phase, Nd-121)

3.2.3.1. Previous studies. The brown phase $Ba_{1+x}Nd_{2-x}CuO_{5-z}$ plays an important role in the processing

Table 5
Nominal lattice parameters for $Ba_{2-x}Nd_{1+x}CuO_{3+z}$ prepared at $pO_2 = 21$ kPa at about 900°C and slowly cooled to room temperature

Composition	a (Å)	b (Å)	c (Å)	V (Å^3)
Ba_2CuO_{3+x}	12.9580(16)	4.0789(6)	3.9101(5)	206.66(4)
$Ba_{1.9}Nd_{0.1}CuO_{3+x}$	12.953(14)	4.030(7)	3.891(4)	203.1(3)
$Ba_{1.8}Nd_{0.2}CuO_{3+x}$	12.960(6)	3.995(2)	3.884(2)	201.12(15)
$Ba_{1.6}Nd_{0.4}CuO_{3+x}$	12.947(15)	3.942(4)	3.853(5)	196.6(3)

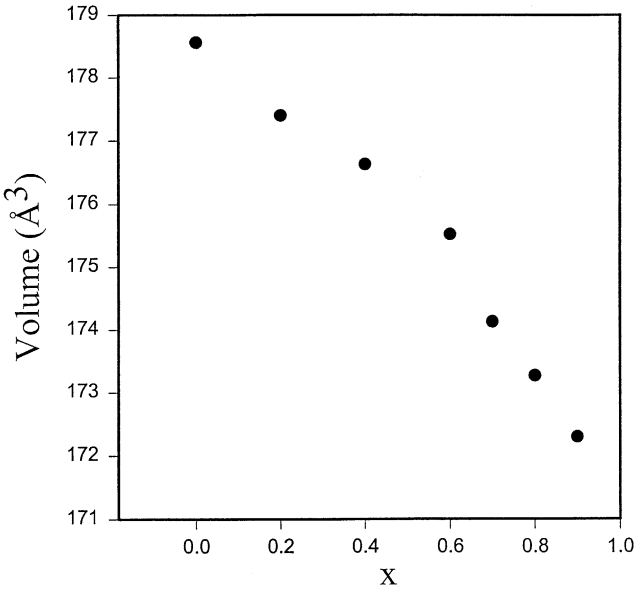

Fig. 9. Plots of unit-cell volume (V) against x in $(Ba_{2-x}Nd_x)CuO_{3+z}$ (experiments at $pO_2 = 21$ kPa).

of high T_c R-213 superconductors. This phase is tetragonal $I4/mbm$ [41] as compared to the orthorhombic green phase BaR_2CuO_5 (R = Sm to Lu) [78]. In the brown phase structure, a three-dimensional array of edge- and face-sharing BaO_{10} and NdO_{10} polyhedra is found. The NdO_8 polyhedron is a square prism capped on two of the three rectangular faces; and the BaO_{10} polyhedron is a square prism capped on both ends by tetragonal pyramids. The square planar CuO_4 are discrete units, and are orthogonal to the neighboring CuO_4 units.

The use of the Nd-211 phase and the flux pinning mechanism was reviewed by Murakami et al. [8]. The advantages of the brown phase inclusions on flux penetration in melt-textured $Ba_2NdCu_3O_{6+z}$ superconductors have been discussed by Babu et al. [79]. Pinning effects due to the Nd-121 particles were found by a systematic study of the variation of the Nd-121 content on the magnetic properties of melt processed Nd-213 phase [80]. A remarkable enhancement of the magnetic levitation force of Nd-213 was induced when textured $Nd_4Ba_2Cu_2O_z$ brown particles were homogeneously distributed throughout samples [81]. Microcracks in the samples were also reduced by the 211 particles. The enhancement of the magnetic levitation force is attributed to the suppression of weak links in grains. Kojo et al. [82], using the brown phase as a precursor together with Nd-213, obtained a bulk superconductor with a high T_c (94–95 K) and sharp onset, and high J_c (2.3×10^4 A/cm^2).

3.2.3.2. Current results. The 'brown phase' was confirmed in the present study to be a solid solution series $Ba_{1+x}Nd_{2-x}CuO_z$ ($0 < x < 0.15$ at $pO_2 = 100$ Pa and $0 < x < 0.2$ at $pO_2 = 21$ kPa). The range of solid solution is rather narrow as compared to the $Ba_{2-x}Nd_{1+x}Cu_3O_{6+z}$ series. This phase is in equilibrium with Nd-213, $Ba_4Nd_2Cu_2O_9$, Nd_2CuO_4, $BaNd_2O_4$, Nd_2O_3 and $(Ba,Nd)_2CuO_{3+z}$ (Figs. 2 and 3).

3.2.4. $Ba_4Nd_2Cu_2O_9$ (Nd-422)

The structure of $Ba_4Nd_2Cu_2O_9$ has been determined by both X-ray and electron diffraction methods [42] to be tetragonal with a space group $P\bar{4}n2$. The (001) projection of the $Ba_2NdCuO_{4.5}$ structure is shown in Fig. 10a, and the one-dimensional chains of CuO_5 are shown in Fig. 10b. This semiconductor phase is one of the first cuprate phases reported which possesses unusual one-dimensional chains of CuO_5 units [42]. These distorted and isolated CuO_5 units form corner-shared infinite chains running parallel to the c-axis. The CuO_5 chains are connected via Ba^{2+} and Nd^{3+} cations, which themselves adopt distorted mono-capped trigonal prismatic configurations (NdO_7 and BaO_7). Octagonal tunnels are found throughout the structure. The Nd environment in Nd-422 is rather different from that of the brown phase $BaNd_2CuO_5$ in which the Nd has an eight-fold coordination [41].

The lattice parameters for samples slow cooled at $pO_2 = 100$ Pa and at $pO_2 = 21$ kPa were determined using neutron diffraction to be $a = 11.9505(8)$ Å and $c = 3.8556(2)$ Å; and $a = 12.0854(3)$ Å and $c = 3.8804(1)$ Å, respectively. The expansion of cell parameters in going from reduced to more oxidizing conditions indicates a possible non-stoichiometry of oxygen in the structure. Detailed structural analysis using neutron diffraction will be reported elsewhere.

4. Implications for processing of Nd-213 superconducting materials

From examination of Figs. 2 and 3, the effect of pO_2 on the solid solution range of the Nd-213 superconductor is clear. The much larger homogeneity limit at $pO_2 = 21$ kPa relative to that at $pO_2 = 100$ Pa provides an obvious path for generation of second-phase particles for potential flux-pinning centers. Since the $Ba_{2-x}Nd_{1+x}Cu_3O_{6+z}$ss varies only in the direction

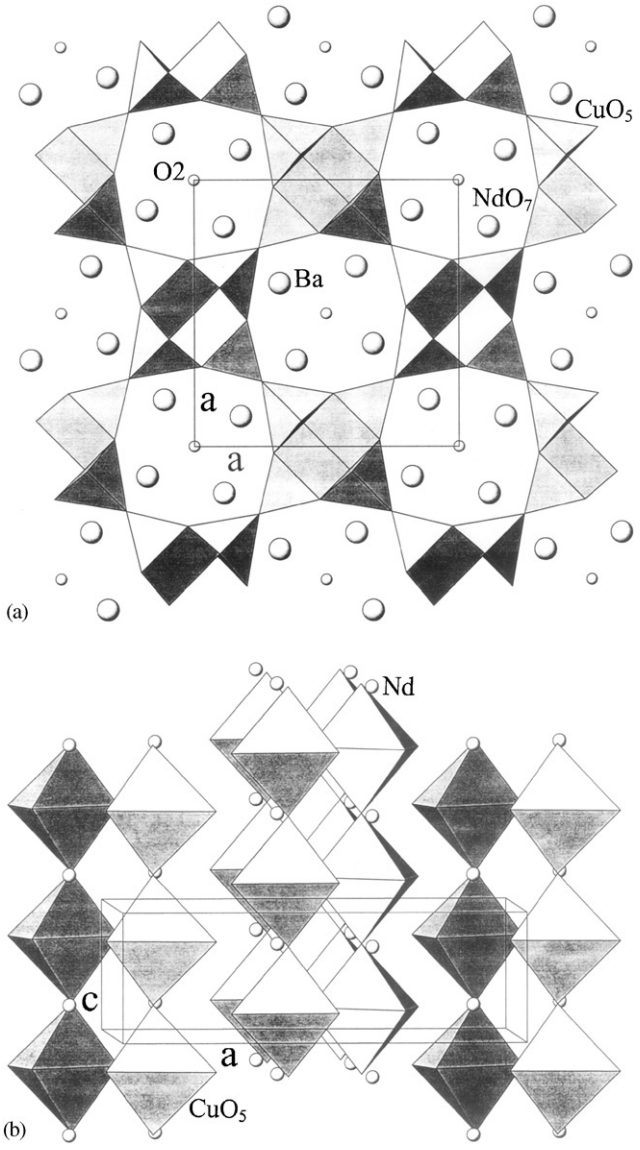

Fig. 10. The structure of the $Ba_4Nd_2Cu_2O_9$ phase showing (a) the (001) projection, and (b) the one-dimensional corner-shared chains of CuO_5 square-pyramids [42].

of the hypothetical end member $Nd_3Cu_3O_{6+z}$ (corresponding to $x = 2$), it follows that by first processing at higher pO_2, and then annealing at lower pO_2, decomposition of homogeneous Nd-213ss to a less Nd-rich 213ss plus Nd_2CuO_4 and CuO_x could result. In principle, this process might be controlled to vary the microstructure of the products in such a way as to tailor the flux-pinning properties. More complicated processing routes could involve, for example, choosing an initial bulk composition such that it fell in the $Ba_{2+x}Nd_{4-x}Cu_2O_z$–Nd-213ss two-phase field at higher pO_2, then finished at lower pO_2 on the Nd_2CuO_4–Nd-213ss tie line, thereby eliminating the CuO_x and leaving only Nd_2CuO_4 as the flux-pinning agent. Other possibilities can be devised, depending on the mix of second- and third-phase particles desired. In contrast to the commonly used processing methods for flux-pinned Y-213, this method avoids the use of liquid.

As noted, there is a significant difference in the tie-line distributions of Figs. 2 and 3 occurring under carbonate-free conditions, relative to those occurring in the phase diagrams based on $BaCO_3$-derived starting materials. Under carbonate-free conditions, over the range of pO_2 investigated in the present study, the $Ba_{2-x}Nd_{1+x}Cu_3O_{6+z}$–$(Ba,Nd)_2CuO_{3+z}$ tie line replaces a $BaCuO_{2+z}$–$Ba_{2+x}Nd_{4-x}Cu_2O_z$ tie line. The net effect of this change is to expand the field of stability of Nd-213ss toward the BaO-corner of the phase diagram. However it is questionable as to whether this is an advantage for Nd-213 processing, since as a result of the tie-line switch, $(Ba,Nd)_2CuO_{3\pm x}$ can now coexist with Nd-213ss. Because $(Ba,Nd)_2CuO_{3+z}$ is atmospherically sensitive, its presence in Nd-213 materials could be deleterious, and it may be important during the RABiTS and IBAD processes to avoid bulk compositions in this region.

5. Summary

Using BaO as a starting reagent, and handling samples under carbonate-free and moisture-free conditions, subsolidus phase diagrams of the system BaO–Nd_2O_3–CuO_x were completed at $pO_2 = 100$ Pa (810°C) and at $pO_2 = 21$ kPa (930°C). The two phase diagrams are similar to each other, except for the different solid solution range. In the BaO-rich region, two phases were observed, namely the orthorhombic $Ba_{2-x}Nd_xCuO_{3+z}$ and the $Ba_4Nd_2Cu_2O_x$ (211) phases. At $pO_2 = 100$ Pa and at $pO_2 = 21$ kPa, the solid solution extent of $Ba_{2-x}Nd_xCuO_{3+z}$ was found to decrease from $x = 0.45$ to 0.3 down to effectively $x = 0$, respectively. The solid solution range of $Ba_{2-x}Nd_{1+x}Cu_3O_{6+z}$ extends from $x = 0$ to ≈ 0.3 at $pO_2 = 100$ Pa, and from $x = 0$ to 0.95 at $pO_2 = 21$ kPa. TEM results suggest the formation of a superlattice in $Ba_{2-x}Nd_{1+x}Cu_3O_{6+z}$ with $x \geqslant 0.7$. Work is in progress to apply both electron and neutron diffraction to elucidate the details of a superstructure in this solid solution series, and the two-phase region between the orthorhombic (O′) and tetragonal (T) solid solution. Results will be reported elsewhere. Phase diagrams of the BaO–R_2O_3–CuO_x systems under controlled-atmosphere conditions and at reduced oxygen partial pressures are important for coated-conductor development, and investigations of other phase diagrams of the lanthanide series are planned.

Acknowledgments

The Department of Energy is acknowledged for partial financial support. The authors are grateful for

the graphical assistance of N. Swanson and P. Schenck. The authors are also grateful for helpful discussions with Drs. Y. Shiohara and T. Izmuri of ISTEC, Japan.

References

[1] A. Goyal, D.P. Norton, J.D. Budal, M. Paranthama, E.D. Specht, D.M. Kroeger, D.K. Christen, Q. He, B. Saffian, F.A. List, D.F. Lee, P.M. Martin, C.E. Klabunde, E. Hartfield, V.K. Sikka, Appl. Phys. Lett. 69 (12) (1996) 1795–1797.

[2] M. Paranthaman, C. Park, X. Cui, A. Goyal, D.F. Lee, P.M. Martin, T.G. Chirayil, D.T. Verebelyi, D.P. Norton, D.K. Christen, D.M. Kroeger, J. Mater. Res. 15 (12) (2000) 2647; Q. He, D.K. Christen, J.D. Budai, E.D. Specht, D.E. Lee, A. Goyal, D.P. Norton, M. Paranthaman, F.A. List, D.M. Kroeger, Physica C 275 (1997) 155–161.

[3] R.P. Reade, P. Berdahl, R.E. Russo, S.M. Garrison, Appl. Phys. Lett. 61 (18) (1992) 2231–2233.

[4] S.R. Foltyn, P. Tiwari, R.C. Dye, M.Q. Le, X.D. Wu, Appl. Phys. Lett. 63 (13) (1993) 1849–1850.

[5] Y. Iijima, N. Tanabe, O. Kohno, Y. Ikeno, Appl. Phys. Lett. 60 (6) (1992) 769–771.

[6] M. Murakami, S.-I. Yoo, T. Higuchi, N. Sakai, J. Welta, N. Koshizuka, S. Tanaka, Jpn. J. Appl. Phys. 33 (5B) (1994) L715.

[7] S.I. Yoo, N. Sakai, H. Takaichi, T. Higuchi, M. Murakami, Appl. Phys. Lett. 65 (5) (1994) 633–635.

[8] M. Murakami, S. Sakai, T. Higuchi, W.I. Yoo, Supercond. Sci. Technol. 9 (1996) 1015.

[9] P. Schätzle, G. Ebbing, W. Bieger, G. Krabbes, Physica C 330 (2000) 19.

[10] R.W. McCallum, J. Metals 41 (1989) 50–52.

[11] M. Kambara, T. Umeda, M. Tagami, X. Yao, E.A. Goodilin, Y. Shiohara, J. Am. Ceram. Soc. 81 (8) (1998) 2116.

[12] K. Oka, M. Saito, M. Ito, K. Nakane, K. Murata, Y. Nishihara, H. Unoki, Jpn. J. Phys. Lett. L219 (1989).

[13] S.F. Xie, S. Liang, G. Che, Z. Zhao, Mod. Phys. Lett. B 2 (9) (1988) 1073.

[14] K. Osamura, W. Zhang, Z. Metallkd. 84 (1993) 8.

[15] E. Goodilin, M. Kambara, T. Umeda, Y. Shiohara, Physica C 289 (1997) 251.

[16] F. Abbattista, D. Mazza, M. Vallino, Eur. J. Solid State Inorg. Chem. 28 (1991) 649.

[17] W. Wong-Ng, L.P. Cook, B. Paretzkin, M.D. Hill, J.K. Stalick, J. Am. Ceram. Soc. 77 (9) (1994) 2354.

[18] S.J. Fu, S.S. Xie, Chin. Sci. Bull. 35 (10) (1990) 816–820.

[19] S.A. Hodorowicz, J. Czerwonka, H.A. Eick, J. Solid State Chem. 88 (1990) 391.

[20] Y. Nakamura, M. Ambara, T. Izumi, Y. Shiohara, Physica C 335 (2000) 56–60.

[21] W. Zhang, K. Osamura, Jpn. J. Appl. Phys. 29 (1990) L1092.

[22] E.A. Goodilin, N.N. Oleynikov, E.V. Antipov, R.V. Shpanchenko, G.Yu. Popov, V.G. Balakirev, Yu.D. Tretyakov, Physica C 272 (1996) 65.

[23] H. Wu, K.W. Dennis, M.J. Kramer, R.W. McCallum, Appl. Supercond 6 (2) (1998) 87.

[24] H. Wu, M.J. Kramer, K.W. Dennis, R.W. McCallum, Physica C 290 (1997) 252.

[25] M. Kambara, M. Nakamura, Y. Shiohara, T. Umeda, Physica C 275 (1997) 237.

[26] T.B. Lindemer, E.D. Specht, P.M. Martin, M.L. Flitcroft, Physica C 255 (1995) 65.

[27] F. Abbattista, C. Brisi, M. Lucco-Borlera, M. Vallino, Nuovo Cimento 10 (1988) 611.

[28] E. Goodilin, M. Kambara, T. Umeda, Y. Shiohara, Physica C 289 (1997) 37.

[29] K. Osamura, W. Zhang, Z. Metallkd. 84 (8) (1993) 522.

[30] J.J. Ritter, Powder Diffract. 3 (1) (1988) 30–31.

[31] R.S. Roth, C.J. Rawn, F. Beech, J.D. Whitler, J.O. Anderson, in: M.F. Yan (Ed.), Ceramic Superconductors II, Amer. Ceram. Soc., Westerville, OH, 1988, pp. 13–26.

[32] S.N. Koshcheeva, V.A. Fotiev, A.A. Fotiev, V.G. Zubkov, Izv. Akad. Nauk SSSR, Neorg. Mater. 26 (7) (1990) 1491; S.N. Koshcheeva, V.A. Fotiev, A.A. Fotiev, V.G. Zubkov, Inorg. Mater. 26 (7) (1990) 1267.

[33] D.M. Deelewee, C.A.H.A. Mutasers, C. Langereis, H.C.A. Smoorenburg, P.J. Pommers, Physica C 152 (1) (1988) 39–49.

[34] S.I. Yoo, R.W. McCallum, Physica C 210 (1993) 147–156.

[35] G.A. Costa, M. Ferretti, M.L. Fornasini, E.A. Franceschi, G.L. Olcese, Powder Diffract. 4 (1989) 12.

[36] H. Muller-Buschbaum, Z. Anorg. Chem. 358 (1968) 138.

[37] A. Apostolov, G. Gassi, God. Sofii. Univ. Fiz. Fak. 63 (1971) 177.

[38] W. Wong-Ng, B. Paretzkin, Powder Diffract. 6 (4) (1991) 187.

[39] N.E. Brese, M. O'Keeffe, Acta Crystallogr. B 47 (1991) 192.

[40] I.D. Brown, D. Altermat, Acta Crystallogr. B 41 (1985) 244–247.

[41] J. Stalick, W. Wong-Ng, Mater. Lett. 9 (10) (1990) 401.

[42] B. Domenges, F. Abbattista, C. Michel, M. Vallino, L. Barbey, N. Nguyen, B. Raveau, J. Solid State Chem. 106 (1993) 271.

[43] A.K. Cheetham, B.E.F. Fender, M.J. Cooper, J. Phys. C 4 (1971) 3107.

[44] C. Challiout, Mater. Res. Soc. Symp. Proc. 169 (1990) 47.

[45] D. Babel, E. Herdweck, Z. Anorg. Allg. Chem. 487 (1982) 75.

[46] W. Wong-Ng, B. Paretzkin, E. Fuller Jr., J. Solid State Chem. 84 (1990) 117.

[47] T. Ishiguro, J. Solid State Chem. 49 (1983) 232.

[48] H.U. Koehler, M. Jansen, Z. Anorg. Allg. Chem. 543 (1986) 73.

[49] W. Wong-Ng, L.P. Cook, Powder Diffract. 9 (4) (1994) 280.

[50] S. Petricek, N. Bukovec, P. Bukovec, J. Solid State Chem. 99 (1992) 58.

[51] W. Wong-Ng, K. Davis, R.S. Roth, J. Am. Ceram. Soc. 71 (2) (1988) C64.

[52] M.T. Weller, D.R. Lines, J. Solid State Chem. 82 (1989) 21.

[53] D.W. Deleeuw, C.A. Mutsaer, C. Langereis, H.C. Smoorenburg, P.J. Rommers, Physica C 152 (1988) 39.

[54] J. Thompson, J.D. FitzGerald, R.L. Withers, P.J. Barlov, J.S. Anderson, Mater. Res. Bull. 24 (1989) 505.

[55] G.F. Voronin, S.A. Degterev, J. Solid State Chem. 110 (1994) 50.

[56] W. Wong-Ng, L.P. Cook, J. Am. Ceram. Soc. 77 (7) (1995) 1883.

[57] W. Wong-Ng, L.P. Cook, J. Res. Natl. Inst. Stand. Technol. 103 (1998) 379.

[58] Chr.L. Teske, Hk. Muller-Buschbaum, Z. Anorg. Allg. Chem. 379 (1970) 113.

[59] M.J. Kramer, S.I. Yoo, R.W. McCallum, Physica C 219 (1994) 145.

[60] M.J. Kramer, S.I. Soo, R.W. McCallum, W.B. Yelonm, H. Xie, P. Allenspach, Physica C 219 (1994) 145.

[61] M.J. Kramer, A. Karion, K.W. Dennis, M. Park, R.W. McCallum, J. Electron. Mater. 23 (11) (1994) 1117.

[62] R.D. Shannon, C.T. Prewitt, Acta Crystallogr. 25 (1969) 925.

[63] R.D. Shannon, Acta Crystallogr. A 32 (1976) 751.

[64] E. Goodilin, M. Limonov, A. Panfilov, N. Khasanova, A. Oka, S. Tajima, Y. Shiohara, Physica C 300 (1998) 250.

[65] M. Yoshizumi, M. Kambara, Y. Shiohara, T. Umeda, Physica C 334 (2000) 77–86.

[66] W. Wong-Ng, L.P. Cook, C.K. Chiang, L.J. Swartzendruber, L.H. Bennett, J.E. Blendell, D. Minor, J. Mater. Res. 3 (5) (1988) 832.

[67] W. Wong-Ng, L.P. Cook, C.K. Chiang, L.J. Swartzendruber, L.H. Bennett, in: M.F. Yan (Ed.), Ceramic Superconductors II, American Ceramic Society, Westerville, OH, 1988, p. 27.

[68] W. Wong-Ng, L.P. Cook, C.K. Chiang, M.D. Vaudin, D.L. Kaiser, F. Beech, L.J. Swartzendruber, L.H. Bennett, E.R. Fuller, in: S.H. Whang, A. GasGupta (Eds.), Proceedings of the 1989 TMS Symposium on High Temperature Superconducting Compounds: Processing & Related Properties, Las Vegas, NV, 1989, The Metallurgical Society, Warrendale, PA, 1989, p. 533.
[69] Y.D. Tretyakov, E.Z. Goodilin, Russ. Chem. Rev. 69 (1) (2000) 1–34.
[70] V.V. Petrykin, P. Berastegul, M. Kakihana, Chem. Mater. 11 (1999) 3445–3451.
[71] S. Takekawa, H. Nozaki, Y. Ishizawa, N. Iyi, Jpn. J. Appl. Phys 26 (12) (1987) L2076.
[72] S.I. Yoo, R.W. McCallum, Physica C 210 (1993) 157.
[73] M. Murakami, S.I. Yoo, T. Higuchi, N. Sakai, M. Wathiki, N. Koshizuk, S. Tanaka, Physcia C 235–40 (1994) 2781.
[74] Y. Shiohara, E.A. Goodilin, in: K.A. Gschneidner Jr., L. Eyring, M.B. Maple (Eds.), Handbook on the Physics and Chemistry of Rare Earths, Vol. 30, Elsevier Science BV, Amsterdam, 2000, pp. 67–227 (Chapter 189).
[75] D.E. Appleman, H.T. Evans, Jr., Report PB216188, US Department of Commerce, National Technical Information Service, 5285 Port Royal Rd., Springfield, VA, 22151.
[76] W. Wong-Ng, C.K. Chiang, B. Paretzkin, E.R. Fuller Jr, Powder Diffract. 5 (1) (1990) 26–32.
[77] W. Wong-Ng, M. Kuchinskin, B. Paretzkin, H.F. McMurdie, Powder Diffract. 4 (1) (1989) 2.
[78] C.L. Teske, H. Muller-Buschbum, Z. Anorg. Allg. Chem. 379 (1970) 234.
[79] N.H. Babu, T. Rajasekharan, V.S. Bai, Physica C 302 (1998) 167.
[80] N.H. Babu, T. Rajasekharan, L. Menon, S. Srinivas, S.K. Malik, Physica C 305 (1998) 103.
[81] A.M. Hu, Z.X. Zha, J.W. Xiong, C. Pang, Physica C 288 (1997) 136.
[82] H. Kojo, S.I. Yoo, M. Murakami, Physica C 289 (1997) 85.
[83] X. Yao, M. Kambare, T. Meda, Y. Shiohara, Physica C 296 (1998) 69.